

# Optimal experiment design for physiological parameter estimation using hyperpolarized carbon-13 magnetic resonance imaging

John Maidens, Peder E. Z. Larson and Murat Arcak

**Abstract**—Hyperpolarized carbon-13 magnetic resonance imaging is a new medical imaging modality that has enabled the real-time observation of perfusion and metabolism in vivo. The rates at which perfusion and metabolism occur are important for disease diagnosis and treatment monitoring. To generate an image, the user must choose a flip angle at which to perturb the magnetic spins associated with each of the compounds to be imaged. We consider the problem of optimally choosing a time-varying sequence of flip angles in order to achieve the best estimates of rate parameters in a physiological model. We first formulate a discrete-time model describing perfusion, exchange, relaxation and measurement error. We then show how to compute the Fisher information for the unknown parameters of this model and present time-varying flip angle schemes that maximize the Fisher information. Through numerical studies, we demonstrate that the optimal flip angle scheme provides better estimates of the model’s rate parameters than a constant flip angle scheme.

## I. INTRODUCTION

Recently-developed techniques for hyperpolarizing carbon-13-containing organic molecules [1] have allowed new insight into perfusion and metabolism through hyperpolarized  $^{13}\text{C}$  magnetic resonance imaging (MRI) and spectroscopy (MRS) [2]. MRI and MRS can be used to generate in vivo measurements of hyperpolarized compounds such as  $^{13}\text{C}$ -labeled pyruvate along with its metabolic products such as lactate. This enables the quantitative estimation of physiological parameters such as perfusion and reaction rates, which can be used to diagnose cancer and monitor its response to treatment [3]. The first clinical trial using hyperpolarized carbon-13 MRI was recently completed in prostate cancer patients [4]. It demonstrated the safety and feasibility of this technique in humans, and showed elevated metabolic conversion from hyperpolarized  $^{13}\text{C}$ -pyruvate to  $^{13}\text{C}$ -lactate in tumors.

In contrast with conventional imaging, in hyperpolarized MRI, magnetization is a non-renewable resource. Conventional MRI measures the magnetization of hydrogen, which is plentiful in the body, and thus at thermal equilibrium there is enough magnetization to produce measurable amount of signal. This allows an arbitrary number of acquisitions to be performed if we allow time for the magnetization to return to equilibrium between acquisitions. In contrast, the thermal

equilibrium magnetization of  $^{13}\text{C}$  is much smaller than hydrogen due to its lower concentration and gyromagnetic ratio.  $^{13}\text{C}$  MRI would be very valuable because of the important role of carbon in biology, but this is nearly impossible due to the low equilibrium magnetization. Hyperpolarization has enabled generation of high-quality  $^{13}\text{C}$  MRI signals. Hyperpolarization can only be performed before the  $^{13}\text{C}$ -labeled compound (*e.g.* pyruvate) is injected into the body, and once injected the magnetization decays over time and is partially destroyed when acquisitions are made. Thus, it is important to carefully choose how acquisitions are made, to make the best use of the limited magnetization available.

In current practice a constant flip angle sequence is used, with the flip angle chosen arbitrarily by the user. Typical values range from 10–30 degrees. Our goal is to choose a time-varying flip angle sequence  $\theta$  that manages the trade-off between present and future measurement quality by maximizing the information about the unknown parameters contained in the acquired data. We do so by presenting an optimal experiment design procedure that maximizes various measures of the Fisher information matrix [5].

We begin in Section II by developing a model of the magnetization dynamics that incorporates perfusion of hyperpolarized pyruvate from the blood to the tissues, the  $T_1$  decay of the magnetization as it relaxes back to equilibrium, and the exchange of magnetization as pyruvate is converted into lactate in the tissues. The model also incorporates measurement error in the form of Rician-distributed noise. In Section III, we discuss optimal experiment design and show how the Fisher information for this model can be computed. In Section IV we present a  $D$ -optimal variable flip angle scheme for simultaneously estimating perfusion and exchange rates, and we compare the variance of the resulting parameter estimates with those resulting from two constant flip angle schemes. In Section V we demonstrate that this technique generalizes easily to more complex models than the two-compartment model from Section II.

To ensure reproducibility of our results, MATLAB code to reproduce all figures in this paper is hosted at <https://github.com/maidens/ACC-2015>.

## II. MODEL

We consider a dynamic model

$$\frac{dx}{dt}(t) = \begin{bmatrix} -k_{PL} - R_{1P} & 0 \\ k_{PL} & -R_{1L} \end{bmatrix} x(t) + \begin{bmatrix} k_{TRANS} \\ 0 \end{bmatrix} u(t) \quad (1)$$

with unknown rate parameters  $R_{1P}$ ,  $R_{1L}$ ,  $k_{PL}$ ,  $k_{TRANS}$  that models the magnetization dynamics in a tissue using an

J. Maidens and M. Arcak are with the Department of Electrical Engineering & Computer Sciences, University of California, Berkeley, 253 Cory Hall, Berkeley, CA, 94720 USA e-mail: {maidens, arcak}@eecs.berkeley.edu. P. Larson is with the Department of Radiology, University of California, San Francisco, 1700 4th St., San Francisco, CA, 94158 USA email: peder.larson@ucsf.edu. Research supported in part by NSERC postgraduate fellowship PGFD3-427610-2012 and NIH grants R00-EB0120164 and P41-EB013598.

arterial input function [6]. The state  $x_1(t)$  denotes the magnetization contained in pyruvate and  $x_2(t)$  the magnetization contained in lactate. The input to the system  $u$  is a measured arterial input function, assumed to be of gamma-variate shape with unknown parameters  $t_0, \alpha, \beta, A_0$  [7].

We acquire data at  $N$  time points separated by intervals of length  $T_R$ . Each time  $t$  an acquisition is made, we must choose a flip angle  $\theta_{k,t}$  for each compound  $k$  to be measured. If the magnetization of the  $k$ -th compound before the acquisition is  $x_k$ , then this choice of flip angle allows us to measure a signal of magnitude  $\sin(\theta_{k,t})x_k$ , after which  $\cos(\theta_{k,t})x_k$  magnetization remains for future acquisitions. This causes discrete jumps, or resets, in the system state, leading to a hybrid dynamical system [8]. Since we are only interested in the system's state at acquisition times, we can avoid technicalities associated with hybrid system modelling by discretizing the system in time and considering a discrete-time dynamical system that simultaneously captures the evolution of (1) between acquisitions and the discrete jumps induced by the acquisitions. We define the transition matrices  $A_d$  and  $B_d$

$$A_d = \exp\left(T_R \begin{bmatrix} -k_{PL} - R_{1P} & 0 \\ k_{PL} & -R_{1L} \end{bmatrix}\right)$$

$$B_d = \begin{bmatrix} -k_{PL} - R_{1P} & 0 \\ k_{PL} & -R_{1L} \end{bmatrix}^{-1} (A_d - I) \begin{bmatrix} k_{TRANS} \\ 0 \end{bmatrix}$$

that correspond to the discretization of dynamics (1) assuming a zero-order hold on the input between each acquisition [9]. The measurements acquired are modelled as Rician-distributed random variables [10], which have probability density

$$f_{x,\sigma}(y) = \frac{y}{\sigma^2} \exp\left(-\frac{y^2 + x^2}{2\sigma^2}\right) I_0\left(\frac{yx}{\sigma^2}\right)$$

where  $I_\nu$  denotes the modified Bessel function of the first kind of order  $\nu$ . Together, these lead to a discrete-time model

$$\begin{aligned} u_t(p) &= A_0(tT_R - t_0)^\alpha e^{-\frac{tT_R - t_0}{\beta}} \\ x_0 &= 0 \\ x_{t+1} &= A_d(p) \begin{bmatrix} \cos\theta_{1,t} & 0 \\ 0 & \cos\theta_{2,t} \end{bmatrix} x_t + B_d(p)u_t(p) \\ \tilde{x}_{k,t} &= \sin(\theta_{k,t})x_{k,t} \quad k = 1, 2 \\ \tilde{x}_{3,t} &= u_t \\ Y_{k,t} &\sim \text{Rice}(\tilde{x}_{k,t}, \sigma_k) \quad k = 1, 2, 3. \end{aligned} \quad (2)$$

To illustrate the data we will work with, simulated trajectories of this model are shown in Figure 1.

The model parameters are

$$p = [R_{1P}, R_{1L}, k_{PL}, k_{TRANS}, t_0, \alpha, \beta, A_0]$$

and we have the freedom to choose

$$q = \begin{bmatrix} \theta_{1,1} & \dots & \theta_{1,N} \\ \theta_{2,1} & \dots & \theta_{2,N} \end{bmatrix}$$

so as to generate the best possible estimate of the unknown parameters. The parameters  $\sigma_k$  for  $k = 1, 2, 3$  can be estimated separately from a measurement of the background

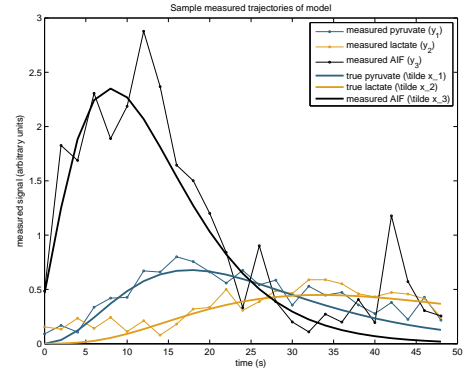


Fig. 1: Simulated output trajectories of the model equations (2).

and are therefore assumed to be known. For now, we fix the repetition time  $T_R = 2$  s, though this could in principle be included in  $q$  as an optimization variable.

### III. OPTIMAL EXPERIMENT DESIGN: METHODS

The optimal design of experiments allows the estimation of model parameters from observed data with minimum variance in the estimates [5]. The Cramér-Rao bound

$$\text{cov}(\hat{p}) \geq \mathcal{I}(p, q)^{-1}$$

gives a lower bound on the covariance of any estimator  $\hat{p}$  in terms of the Fisher information matrix

$$\begin{aligned} \mathcal{I}_{ij}(p, q) &= \mathbb{E} \left[ \frac{\partial \log p(y|p, q)}{\partial p_i} \frac{\partial \log p(y|p, q)}{\partial p_j} \middle| p, q \right] \\ &= \sum_{t=0}^T \sum_{k=1}^3 \mathbb{E} \left[ \frac{\partial \log p(y_{k,t}|p, q)}{\partial p_i} \frac{\partial \log p(y_{k,t}|p, q)}{\partial p_j} \middle| p, q \right]. \end{aligned}$$

It is well known that under mild assumptions, the maximum likelihood estimator is asymptotically efficient [11], that is, it achieves the Cramér-Rao bound as the amount of data collected tends to infinity. Thus, to find a maximum-likelihood estimate with minimum variance, we wish to choose  $q$  in order to maximize the Fisher information matrix at a nominal value of the parameter vector  $p$ .

To formulate this as an optimization problem, we must choose some scalar-valued function of  $\mathcal{I}$  to maximize. Common choices for this function include:

- $f_D(\mathcal{I}) = \det(\mathcal{I})$  ( $D$ -optimal design) which corresponds to minimizing the volume of the estimate's confidence region
- $f_E(\mathcal{I}) = \lambda_{\min}(\mathcal{I})$  ( $E$ -optimal design) which corresponds to minimizing the length of the longest axis of the confidence region
- $f_A(\mathcal{I}) = 1/\text{tr}(\mathcal{I}^{-1})$  ( $A$ -optimal design) which corresponds to minimizing the average length of the confidence region's axes.

### A. Computing the Fisher information matrix

The log likelihood of the observed data for this problem is given by

$$\log p(y_{k,t}|p, q) = \log \left( \frac{y_{k,t}}{\sigma_k^2} \right) - \frac{y_{k,t}^2 + \tilde{x}_{k,t}^2(p, q)}{2\sigma_k^2} + \log I_0 \left( \frac{y_{k,t} \tilde{x}_{k,t}(p, q)}{\sigma_k^2} \right).$$

We can compute its sensitivities with respect to the model parameters as

$$\begin{aligned} \frac{\partial \log p(y_{k,t}|p, q)}{\partial p_i} &= -\frac{\tilde{x}_{k,t}(p, q)}{\sigma_k^2} \frac{\partial \tilde{x}_{k,t}(p, q)}{\partial p_i} \\ &+ \frac{I_1 \left( \frac{y_{k,t} \tilde{x}_{k,t}(p, q)}{\sigma_k^2} \right)}{I_0 \left( \frac{y_{k,t} \tilde{x}_{k,t}(p, q)}{\sigma_k^2} \right)} \frac{y_{k,t}}{\sigma_k^2} \frac{\partial \tilde{x}_{k,t}(p, q)}{\partial p_i} \\ &= -\frac{1}{\sigma_k^2} \frac{\partial \tilde{x}_{k,t}(p, q)}{\partial p_i} \left[ \tilde{x}_{k,t}(p, q) - \frac{I_1 \left( \frac{y_{k,t} \tilde{x}_{k,t}(p, q)}{\sigma_k^2} \right)}{I_0 \left( \frac{y_{k,t} \tilde{x}_{k,t}(p, q)}{\sigma_k^2} \right)} y_{k,t} \right]. \end{aligned}$$

Thus, we can compute

$$\begin{aligned} \mathbb{E} \left[ \frac{\partial \log p(y_{k,t}|p, q)}{\partial p_i} \frac{\partial \log p(y_{k,t}|p, q)}{\partial p_j} \middle| p, q \right] &= \frac{1}{\sigma_k^4} \frac{\partial \tilde{x}_{k,t}(p, q)}{\partial p_i} \frac{\partial \tilde{x}_{k,t}(p, q)}{\partial p_j} \\ &\mathbb{E} \left[ \left( \tilde{x}_{k,t}(p, q) - \frac{I_1 \left( \frac{y_{k,t} \tilde{x}_{k,t}(p, q)}{\sigma_k^2} \right)}{I_0 \left( \frac{y_{k,t} \tilde{x}_{k,t}(p, q)}{\sigma_k^2} \right)} y_{k,t} \right)^2 \middle| p, q \right] \\ &= \frac{1}{\sigma_k^4} \frac{\partial \tilde{x}_{k,t}(p, q)}{\partial p_i} \frac{\partial \tilde{x}_{k,t}(p, q)}{\partial p_j} \left( \tilde{x}_{k,t}^2(p, q) - 2\tilde{x}_{k,t}(p, q)\mathbb{E}_{k,t} + \tilde{\mathbb{E}}_{k,t} \right) \end{aligned}$$

where

$$\begin{aligned} \mathbb{E}_{k,t} &= \mathbb{E} \left[ \frac{I_1 \left( \frac{y_{k,t} \tilde{x}_{k,t}(p, q)}{\sigma_k^2} \right)}{I_0 \left( \frac{y_{k,t} \tilde{x}_{k,t}(p, q)}{\sigma_k^2} \right)} y_{k,t} \middle| p, q \right] \\ &= \int_0^\infty \frac{I_1 \left( \frac{y \tilde{x}_{k,t}(p, q)}{\sigma_k^2} \right)}{I_0 \left( \frac{y \tilde{x}_{k,t}(p, q)}{\sigma_k^2} \right)} y \frac{y}{\sigma_k^2} \exp \left( -\frac{y^2 + \tilde{x}_{k,t}^2(p, q)}{2\sigma_k^2} \right) \\ &\quad I_0 \left( \frac{y \tilde{x}_{k,t}(p, q)}{\sigma_k^2} \right) dy \\ &= \frac{1}{\sigma_k^2} \int_0^\infty y^2 \exp \left( -\frac{y^2 + \tilde{x}_{k,t}^2(p, q)}{2\sigma_k^2} \right) I_1 \left( \frac{y \tilde{x}_{k,t}(p, q)}{\sigma_k^2} \right) dy \\ &= \tilde{x}_{k,t}(p, q) \end{aligned}$$

(see eq. 2.15.5.4 with  $\alpha = \nu + 2$  from [12]) and

$$\begin{aligned} \tilde{\mathbb{E}}_{k,t} &= \mathbb{E} \left[ \left( \frac{I_1 \left( \frac{y_{k,t} \tilde{x}_{k,t}(p, q)}{\sigma_k^2} \right)}{I_0 \left( \frac{y_{k,t} \tilde{x}_{k,t}(p, q)}{\sigma_k^2} \right)} y_{k,t} \right)^2 \middle| p, q \right] \\ &= \int_0^\infty \left( \frac{I_1 \left( \frac{y \tilde{x}_{k,t}(p, q)}{\sigma_k^2} \right)}{I_0 \left( \frac{y \tilde{x}_{k,t}(p, q)}{\sigma_k^2} \right)} y \right)^2 \frac{y}{\sigma_k^2} \exp \left( -\frac{y^2 + \tilde{x}_{k,t}^2(p, q)}{2\sigma_k^2} \right) \\ &\quad \mathcal{I}_0 \left( \frac{y \tilde{x}_{k,t}(p, q)}{\sigma_k^2} \right) dy \\ &= \frac{1}{\sigma_k^2} \int_0^\infty y^3 \frac{I_1^2 \left( \frac{y \tilde{x}_{k,t}(p, q)}{\sigma_k^2} \right)}{I_0 \left( \frac{y \tilde{x}_{k,t}(p, q)}{\sigma_k^2} \right)} \exp \left( -\frac{y^2 + \tilde{x}_{k,t}^2(p, q)}{2\sigma_k^2} \right) dy. \end{aligned}$$

Thus we see that  $\frac{1}{\sigma^2} \left( \tilde{x}_{k,t}^2(p, q) - 2\tilde{x}_{k,t}(p, q)\mathbb{E}_{k,t} + \tilde{\mathbb{E}}_{k,t} \right)$  can be expressed as a function  $\phi$  depending only on the signal-to-noise ratio  $\frac{\tilde{x}_{k,t}(p, q)}{\sigma}$ . This function, defined as

$$\begin{aligned} \phi(z) &= -z^2 + \int_0^\infty y^3 \frac{I_1^2(yz)}{I_0(yz)} \exp \left( -\frac{1}{2}(y^2 + z^2) \right) dy \\ &= -z^2 + \frac{1}{z} \int_0^\infty \log I_0(yz) y^2 \exp \left( -\frac{1}{2}(y^2 + z^2) \right) \\ &\quad \left( (y^2 - 3)I_1(yz) - \frac{1}{2}yz(I_0(yz) + I_2(yz)) \right) dy \end{aligned}$$

is difficult to compute analytically, but for our purposes it is sufficient to evaluate it numerically. In Figure 2, we plot  $\phi$  for various values of the signal-to-noise ratio.

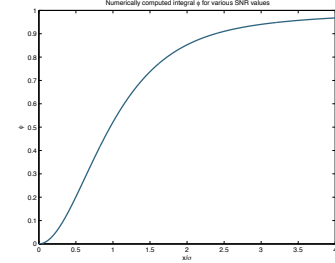


Fig. 2: Values of the function  $\phi$  computed by numerical integration.

Now all that remains in order to compute the Fisher information is to compute sensitivities  $\frac{\partial x_{k,t}}{\partial p_i}(p, q)$ . Using the product rule, we get a recursive formula for the sensitivities

$$\begin{cases} \frac{\partial x_0}{\partial p_i} = 0 \\ \frac{\partial x_{t+1}}{\partial p_i} = \frac{\partial A_d}{\partial p_i} \cos \theta_t x_t + A_d \cos \theta_t \frac{\partial x_t}{\partial p_i} + \frac{\partial B_d}{\partial p_i} u_t + B_d \frac{\partial u_t}{\partial p_i}. \end{cases} \quad (3)$$

Together, we can now compute the  $(i, j)$ -th entry of the Fisher information matrix as

$$\begin{aligned} \mathcal{I}_{ij}(p, q) &= \sum_{t=0}^T \sum_{k=1}^3 \mathbb{E} \left[ \frac{\partial \log p(y_{k,t}|p, q)}{\partial p_i} \frac{\partial \log p(y_{k,t}|p, q)}{\partial p_j} \middle| p, q \right] \\ &= \sum_{t=0}^T \sum_{k=1}^3 \frac{1}{\sigma_k^2} \frac{\partial \tilde{x}_{k,t}(p, q)}{\partial p_i} \frac{\partial \tilde{x}_{k,t}(p, q)}{\partial p_j} \phi \left( \frac{\tilde{x}_{k,t}(p, q)}{\sigma_k} \right) \end{aligned}$$

### B. Eliminating nuisance parameters

Note that we do not necessarily need good estimates of all the unknown parameters in the model. For example, the goal of a particular experiment might be to simultaneously estimate the perfusion parameter  $k_{TRANS}$  and the exchange parameter  $k_{PL}$ , which are useful for discriminating between cancerous and non-cancerous tissues [13]. Thus we wish to modify our optimality criterion to maximize the sensitivity of the experiments to  $k_{PL}$  and  $k_{TRANS}$  while considering the nuisance parameters only insofar as they allow us to estimate the parameters of interest. We do so by partitioning the information matrix as

$$\mathcal{I} = \begin{bmatrix} \mathcal{I}_{11} & \mathcal{I}_{12} \\ \mathcal{I}_{21} & \mathcal{I}_{22} \end{bmatrix}$$

where the first block corresponds to the parameters of interest and the second block corresponds to the nuisance parameters.

Optimal design can be performed by maximizing a scalar-valued function of the Schur complement of  $\mathcal{I}_{22}$  in  $\mathcal{I}$ :

$$\mathcal{S} = \mathcal{I}_{11} - \mathcal{I}_{12}\mathcal{I}_{22}^{-1}\mathcal{I}_{21}$$

(see Section 6.1 of [14]).

### C. Numerical optimization

To design an optimal flip angle scheme, we must solve the flip angle optimization problem

$$\text{maximize}_q f(\mathcal{S}(p, q))$$

for the optimization variable  $q$  where  $f$  is some scalar-valued, order-preserving function such as the  $D$ -,  $E$ - and  $A$ -optimal design criteria, and  $p$  is fixed to some nominal value for the unknown parameters. We do so using the MATLAB Optimization Toolbox [15]. This toolbox provides a derivative-free implementation of the quasi-Newton optimization algorithm of Broyden-Fletcher-Goldfarb-Shanno [16], which is well-suited to finding local minima of our objective function.

## IV. OPTIMAL EXPERIMENT DESIGN: RESULTS

In order to demonstrate our method for optimal flip angle design, we consider an experiment in which we wish to compute estimates of the parameters  $[k_{PL}, k_{TRANS}]$ . To ensure practical identifiability of the unknown parameters, we assume that the parameters  $[R_{1P}, R_{1L}, t_0]$  are known constants with values  $[1/35, 1/30, 0]$  respectively. This is a reasonable assumption as the magnetization decay rates  $R_{1P}$  and  $R_{1L}$  do not vary between patients as much as the other parameters  $k_{PL}, k_{TRANS}, \alpha, \beta$  and  $A_0$ . The nuisance parameters, whose values are unknown but not important to estimate, are  $[\alpha, \beta, A_0]$ . We design an optimal experiment based on the nominal parameter values  $[k_{PL}, k_{TRANS}, \alpha, \beta, A_0] = [0.05, 0.04, 2.00, 5.00, 1.00]$ . We further assume Rician noise with  $[\sigma_1^2, \sigma_2^2, \sigma_3^2] = [0.01, 0.01, 0.1]$ .

### A. Constant flip angle scheme

We first consider the one-dimensional optimization problem of choosing a constant flip angle  $\theta_{k,t} = \theta$  for all  $k, t$ . In Figure 3, we plot three choices of objective function corresponding to the  $D$ -,  $E$ - and  $A$ -optimal design criteria described in Section III. We see that all three objective functions are quasiconcave, allowing their maximum to be easily found. However, the optimal values differ significantly between the three objectives.

### B. Variable flip angle scheme

We now consider a problem in which flip angles can be chosen independently for each of the measured states and inputs and are allowed to vary with time. We define the optimization vector

$$q = [\theta_{k,t} \quad t = 1, \dots, N \quad k = 1, 2].$$

An optimal flip angle scheme for the  $D$ -optimal design criterion is shown in Figure 4.

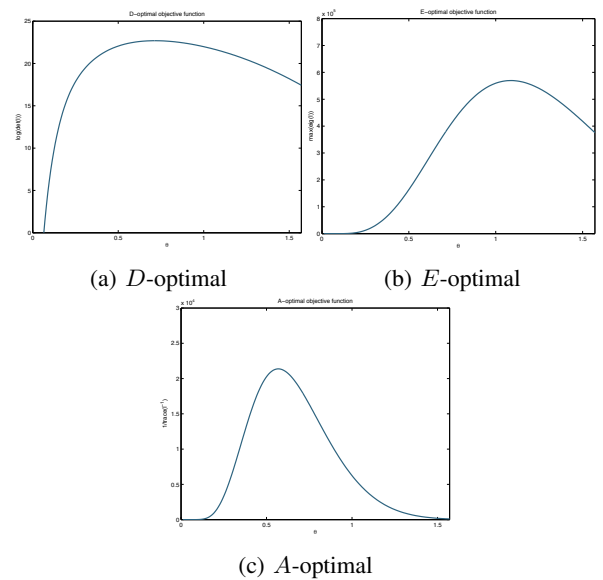


Fig. 3: Comparison of objective functions for the constant flip angle design problem, with nuisance parameters eliminated

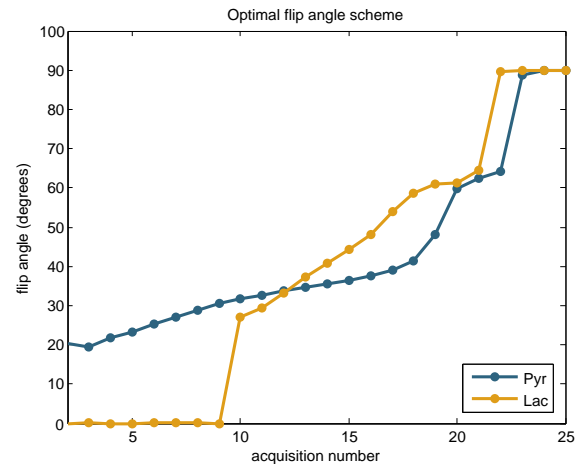
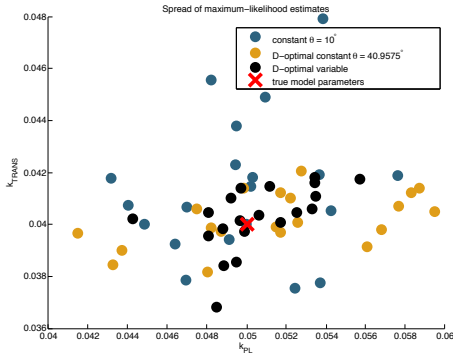


Fig. 4:  $D$ -optimal variable flip angle scheme computed for two-site exchange model.

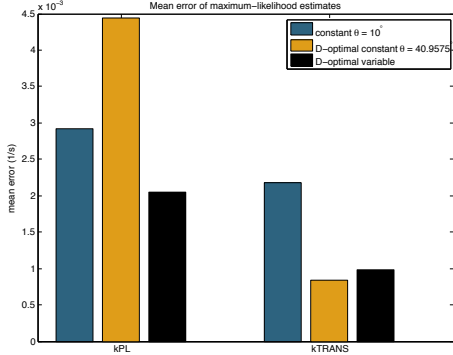
### C. Comparison of flip angle schemes

To demonstrate the advantage of using variable flip angle schemes, we compare maximum likelihood estimates of parameter values resulting from three schemes: a constant flip angle scheme with  $\theta = 10^\circ$ , the  $D$ -optimal constant flip angle scheme with  $\theta_D^* = 40.96^\circ$  and the variable flip angle scheme shown in Figure 4. In Figure 5a, for each of the three flip angle schemes, we plot the spread of maximum likelihood estimates in parameter space corresponding to  $n = 20$  simulated samples of the variable  $Y$ . In Figure 5b, we compare the mean error of the estimates computed as  $e_j = \frac{1}{n} \sum_{i=1}^n |p_j - \hat{p}_{i,j}|$  where  $\hat{p}_{i,j}$  is the  $j$ -th component of the maximum likelihood estimate of the parameter vector  $p$  that is computed using the  $i$ -th sample of the variable  $Y$ .

We see that the  $D$ -optimal solution for the constant flip angle problem is able to significantly improve the estimate of



(a) Comparison of spread in parameter space



(b) Comparison of mean error of estimates

Fig. 5: Comparison of the maximum-likelihood parameter estimates for three flip angle schemes

the perfusion rate  $k_{TRANS}$  compared to the naively-chosen flip angle  $\theta = 10^\circ$ . This is done however at the expense of the quality of the estimate of  $k_{PL}$ . By using a  $D$ -optimal time-varying flip angle scheme, we are able to decrease the estimation error in  $k_{TRANS}$  and  $k_{PL}$  simultaneously compared with the constant scheme with  $\theta = 10^\circ$ .

#### D. Nonuniqueness of local maximum for variable flip angle design problem

In this section, we demonstrate that multiple local equilibria exist for this nonconvex optimization problem. However, since these flip angle protocols are designed offline, it is possible to invest a significant amount of time searching for optima if desired.

In order to test whether the objective function  $f_D(\mathcal{I}(q))$  has a unique maximum, we perform the optimization from a number of initial values. This comparison is shown in Figure 6. For each flip angle scheme, the negative of the  $D$ -optimal objective function value is shown in the subfigure title (here, lower objective function values mean higher information as the MATLAB optimization toolbox defaults to minimizing functions). Subfigures in each row result from the same initialization, but run for differing numbers of iterations.

These results suggest that for acquisitions 2 through 15, where the SNR is high, the locally optimal flip angles found

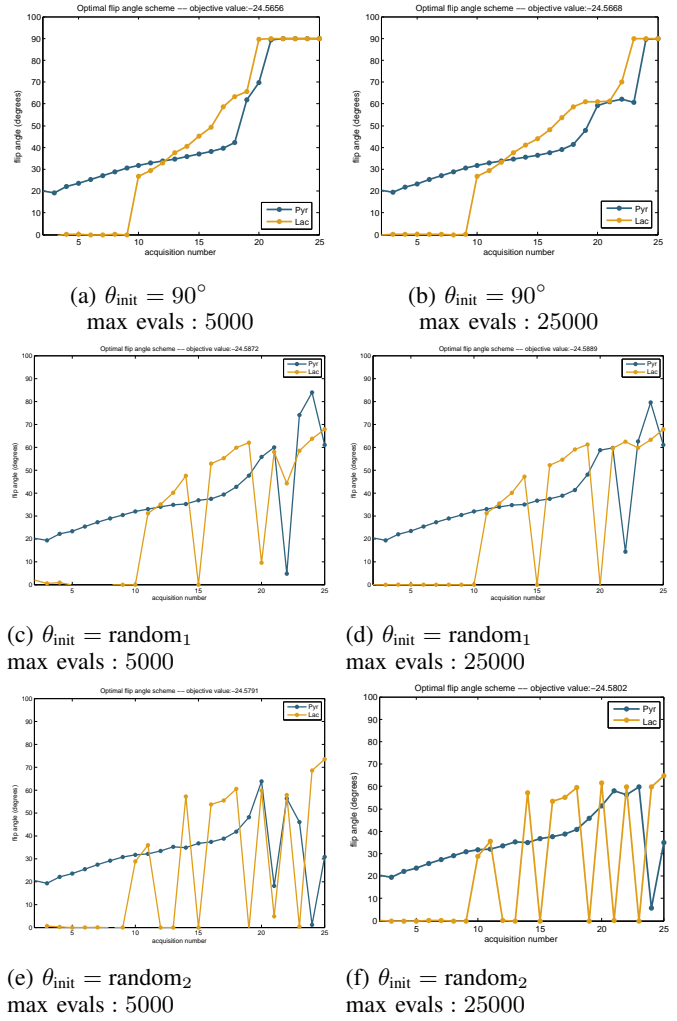


Fig. 6: Comparison of optimal flip angle schemes found using various initializations of the decision variable  $\theta$ .

for pyruvate are very similar for all three initializations. It is only when the SNR drops to a low value that the different optima disagree. Further, the optimal flip angle schemes resulting from all three initializations have very similar values for the objective function. Thus, in this example it is unimportant which local maximum is attained.

#### V. EXTENSION TO MORE GENERAL MODELS

This procedure is not limited to the particular model (1) that we chose, but works equally well for other linear models of exchange, perfusion and relaxation. Indeed, the derivation of the Fisher information given in Section III-A does not depend on the specific dynamics chosen until the recursive formula (3). Thus it is easy to extend these results to a more general class of models.

As an example, we consider the three-site model from [17]

$$\frac{dx}{dt}(t) = \begin{bmatrix} -k_{PL} - k_{PA} - R_{1P} & 0 & 0 \\ k_{PL} & -R_{1L} & 0 \\ k_{PA} & 0 & -R_{1A} \end{bmatrix} x(t) + \begin{bmatrix} k_{TRANS} \\ 0 \\ 0 \end{bmatrix} u(t) \quad (4)$$

where the state  $x_3(t)$  represents the magnetization in the metabolite alanine. The parameter  $k_{PA}$  is added to the set



of parameters of interest and optimization is performed using the nominal value 0.03. The parameter  $R_{1A}$  is assumed to be a known constant with value  $1/40$ . A  $D$ -optimal flip angle scheme for this three-site model is shown in Figure 7.

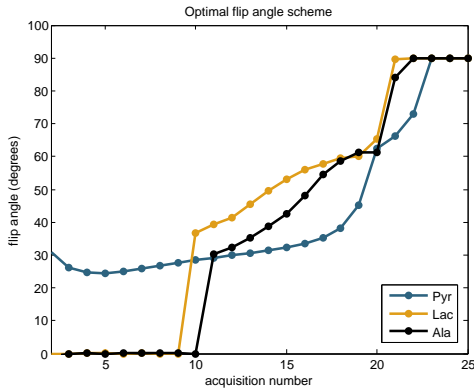


Fig. 7:  $D$ -optimal variable flip angle scheme computed for three-site exchange model.

It may also be the case that the arterial input function must also be estimated from a blood compartment in the image, using the same flip angles as the first compartment. In this case, the model output can be modified by as

$$\tilde{x}_{3,t} = \sin(\theta_{1,t})u_t.$$

The resulting optimal flip angle scheme for the two-compartment model is given in Figure 8.

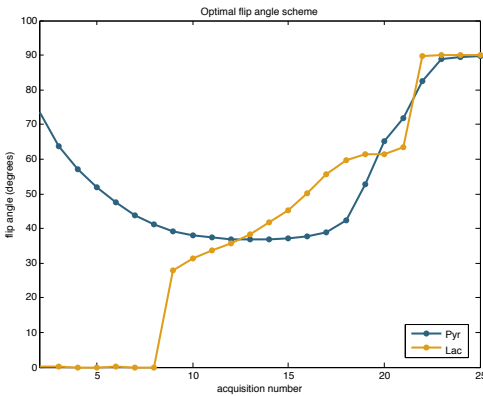


Fig. 8:  $D$ -optimal variable flip angle scheme for the two-site exchange model computed subject to the constraint that flip angles for the first compartment and the input must be equal.

## VI. CONCLUSION

We have formulated a dynamic model describing perfusion, relaxation, exchange and measurement of magnetization in a living subject, and we have derived a formula for the Fisher information about model parameters contained in the output. This allowed us to compute time-varying flip angle schemes that are locally optimal with respect to the Fisher information. While the optimization problem described is nonconvex, we provide evidence that locally optimal variable

flip angle schemes can outperform any constant flip angle scheme. This optimal variable flip angle scheme can simultaneously decrease the error in estimates of the perfusion and metabolism rates in our model, when compared with a naive flip angle scheme. We also demonstrated how these results generalize easily to more complex models, suggesting that these techniques could be widely applicable for quantitative physiological parameter estimation using hyperpolarized magnetic resonance imaging.

## REFERENCES

- [1] J. H. Ardenkjær-Larsen, B. Fridlund, A. Gram, G. Hansson, L. Hansson, M. H. Lerche, R. Servin, M. Thaning, and K. Golman, "Increase in signal-to-noise ratio of  $> 10,000$  times in liquid-state NMR," *Proceedings of the National Academy of Sciences*, vol. 100, no. 18, pp. 10 158–10 163, Sep. 2003.
- [2] K. Golman and S. J. Petersson, "Metabolic imaging and other applications of hyperpolarized  $^{13}\text{C}^1$ ," *Academic Radiology*, vol. 13, no. 8, pp. 932–942, Aug. 2006.
- [3] S. E. Day, M. I. Kettunen, F. A. Gallagher, D.-E. Hu, M. Lerche, J. Wolber, K. Golman, J. H. Ardenkjær-Larsen, and K. M. Brindle, "Detecting tumor response to treatment using hyperpolarized  $^{13}\text{C}$  magnetic resonance imaging and spectroscopy," *Nature Medicine*, no. 11, pp. 1382–1387, 2007.
- [4] S. J. Nelson, J. Kurhanewicz, D. B. Vigneron, P. E. Z. Larson, A. L. Harzstark, M. Ferrone, M. van Criekinge, J. W. Chang, R. Bok, I. Park, G. Reed, L. Carvajal, E. J. Small, P. Munster, V. K. Weinberg, J. H. Ardenkjær-Larsen, A. P. Chen, R. E. Hurd, L.-I. Odegaardstuen, F. J. Robb, J. Tropp, and J. A. Murray, "Metabolic imaging of patients with prostate cancer using hyperpolarized  $[1-^{13}\text{C}]$ pyruvate," *Science Translational Medicine*, vol. 5, no. 198, p. 198ra108, 2013.
- [5] F. Pukelsheim, *Optimal design of experiments*, ser. Probability and mathematical statistics. Wiley, 1993.
- [6] S. M. Kazan, S. Reynolds, A. Kennerley, E. Wholey, J. E. Bluff, J. Berwick, V. J. Cunningham, M. N. Paley, and G. M. Tozer, "Kinetic modeling of hyperpolarized  $^{13}\text{C}$  pyruvate metabolism in tumors using a measured arterial input function," *Magnetic Resonance in Medicine*, vol. 70, no. 4, pp. 943–953, 2013.
- [7] C. von Morze, P. E. Larson, S. Hu, K. Keshari, D. M. Wilson, J. H. Ardenkjær-Larsen, A. Goga, R. Bok, J. Kurhanewicz, and D. B. Vigneron, "Imaging of blood flow using hyperpolarized  $[^{13}\text{C}]$ urea in preclinical cancer models," *Journal of Magnetic Resonance Imaging*, vol. 33, no. 3, pp. 692–697, 2011.
- [8] W. Haddad, V. Chellaboina, and S. Nersisov, *Impulsive and Hybrid Dynamical Systems: Stability, Dissipativity, and Control*. Princeton University Press, 2006.
- [9] C.-T. Chen, *Linear System Theory and Design*, 3rd ed. New York, NY, USA: Oxford University Press, Inc., 1998.
- [10] H. Gudbjartsson and S. Patz, "The Rician distribution of noisy MRI data," *Magnetic Resonance in Medicine*, vol. 34, no. 6, pp. 910–914, 1995.
- [11] H. Cramér, *Mathematical Methods of Statistics*. Princeton University Press, 1946.
- [12] A. Prudnikov, I. Brychkov, and O. Marichev, *Integrals and Series Volume 2: Special functions*. Gordon and Breach Science Publishers, 1986.
- [13] N. Bahrami, C. L. Swisher, C. V. Morze, D. B. Vigneron, and P. E. Z. Larson, "Kinetic and perfusion modeling of hyperpolarized  $^{13}\text{C}$  pyruvate and urea in cancer with arbitrary RF flip angles," *Quantitative Imaging in Medicine and Surgery*, vol. 4, no. 1, 2014.
- [14] É. Walter and L. Pronzato, *Identification of parametric models from experimental data*, ser. Communications and control engineering. Springer, 1997.
- [15] The MathWorks, Inc., "MATLAB and Optimization Toolbox Release 2013b," Natick, Massachusetts, United States.
- [16] J. Nocedal and S. Wright, *Numerical Optimization*. Springer, 2006.
- [17] C. L. Swisher, P. E. Z. Larson, K. Kruttwig, A. B. Kerr, S. Hu, R. A. Bok, A. Goga, J. M. Pauly, S. J. Nelson, J. Kurhanewicz, and D. B. Vigneron, "Quantitative measurement of cancer metabolism using stimulated echo hyperpolarized carbon-13 MRS," *Magnetic Resonance in Medicine*, vol. 71, no. 1, pp. 1–11, 2014.